Philosophical Magazine,
Vol. 85, No. 36, 21 December 2005, 4445–4464

Taylor & Francis
Taylor & Francis Group

Kinetic analysis of the instability of hollow nanoparticles

A. M. GUSAK*†, T. V. ZAPOROZHETS†,
K. N. TU† and U. GÖSELE‡

†Dept. of Materials Science and Engineering, UCLA, 6531 Boelter Hall,
420 Westwood Plaza, Los Angeles, CA 90095
‡Max Planck Institute of Microstructure Physics, Halle, Germany

(*Received 23 March 2005; in final form 15 August 2005*)

A general method of obtaining hollow nanoparticles by utilizing the Kirkendall effect has been reported recently. We examine here the thermal instability of hollow nanoparticles. The difference of vacancy concentrations at the inner and outer surfaces of a nanoshell will generate an outflux of vacancies and transform it into a solid nanoparticle. Phenomenological as well as kinetic Monte Carlo modeling has been applied to analyse the shrinking kinetics of nanoshells, consisting of either a pure element or an intermetallic compound with large difference of partial diffusivities of the components. Shrinking kinetics and time to collapse to solid particles are demonstrated to be determined mainly by the slow diffusant, making compound nanoshells more stable than anticipated.

1. Introduction

Recently, a method of producing hollow nanoparticles, based on the Kirkendall effect [1], was reported [2]. Reaction of nanosize Co particles in S or O_2/Ar ambient lead to the formation of hollow Co_3S_4 and CoO nano particles, respectively. Assuming that Co is the faster diffusing species in the reactions, the in-flux of vacancies into a confined nanoshell of Co_3S_4 or CoO will form a hollow nanoparticle. While this method opens a new direction in manufacturing nanoscale materials, it has been noticed [3] that such nanoshells or nanovoids structure should be unstable. It is energetically favourable for a nanoshell to shrink into a compact nanosphere:

$$\gamma \cdot \left(4\pi r_{i0}^2 + 4\pi r_{e0}^2\right) > \gamma \cdot 4\pi r_f^2, \tag{1}$$

(γ – surface tension, r_{i0}, r_{e0} – initial inner and external radii of nanoshell, r_f – final radius of collapsed particle), with conservation of volume implying: $(4\pi/3)(r_{e0}^3 - r_{i0}^3) = (4\pi/3)r_f^3$.

The proposed atomistic mechanism of shrinking is the vacancy flux from the inner surface (with radius r_i) to the external surface (with radius r_e). The driving force

*Corresponding author. Email: gusak@cdu.edu.ua

Philosophical Magazine
ISSN 1478–6435 print/ISSN 1478–6443 online
http://www.tandf.co.uk/journals
DOI: 10.1080/14786430500311741

of the vacancy flux is the difference of vacancy/atoms chemical potentials and corresponding difference of equilibrium vacancy concentrations at the curved interfaces, $C_V(r_i) > C_V(r_e)$. This Gibbs–Thomson effect can be expressed, in linear approximation so far, as

$$\begin{aligned} C_V(r_i) &= C_V^{eq} \cdot \left(1 + \frac{\beta}{r_i}\right), \\ C_V(r_e) &= C_V^{eq} \cdot \left(1 - \frac{\beta}{r_e}\right), \end{aligned} \tag{2}$$

with $\beta = (2\gamma\Omega/kT)$, Ω – atomic volume, concentration C meaning the fraction of vacant lattice sites. C_V^{eq} refers to the equilibrium concentration of vacancies with respect to a planar surface. The linear approximation holds if $r_i \gg \beta$. If the term β/r becomes comparable with unity, we'll need to reformulate equation (2) using the exponential size dependencies.

Thus, for the case of nanoshells of a single element the physical picture of shrinking seems very clear. It is analogous to the LSW theory of caking [4], when voids are dissolved by vacancy fluxes to external surface. Yet, in the nanoshell case it has a much more symmetrical picture: vacancies are generated at the inner surface (void dissolution), migrate to the external surface, causing the in-flux of atoms and movement of the inner surface, and annihilate at the external surface, causing shrinking of the latter.

In case of a binary alloy or intermetallic compound (IMC) nanoshell, the process is more complicated due to the "inverse Kirkendall effect" [5], which was discussed in the problem of irradiation of an alloy with energetic particles. Since in an alloy or intermetallic, one of the components may diffuse much faster than the other ($D_B \gg D_A$), the vacancy flux should lead to a redistribution of the components – segregation of B-atoms at the inner boundary, and of A-atoms near the external surface. The arising concentration gradient $\partial C_B/\partial r$ will influence and reduce the vacancy flux and hence will generate a tendency to suppress the shrinking process. We will deduce below that the slower diffusing specie will control the shrinking rate. Moreover, segregation is approximately inversely proportional to the square of the inner radius. It means that sooner or later the concentration of B at the inner radius will exceed the homogeneity limit of the IMC, and pure B component can precipitate at the void/IMC interface. After this the shrinking should proceed further, ending with tiny pure B nanoball inside an inhomogeneous (with concentration gradient inside) IMC nanoshell. This kinetic process will be discussed in detail later. To develop the kinetic equations, we shall use the formalism of the classic Darken analysis of interdiffusion and take into account the non-equilibrium vacancies in the interdiffusion. This formalism follows what was developed first by Nazarov and Gurov [6] and later modified by Gurov and Gusak [7–9].

Here we present 4 models of the shrinking of hollow nanospheres with increasing degree of complexity. Model 1 (subsection 2.1) describes the shrinking kinetics of single element nanoshell in steady-state approximation for vacancies. Model 2 (subsection 2.2) describes the shrinking of a binary compound nanoshell in steady-state approximation both for vacancies and for B-species, taking into account the inverse Kirkendall effect. We will demonstrate that the steady-state approximation

is good for vacancies, but not so well justified for the slow-diffusing B-component. Therefore in Model 3 (subsection 2.3) we present a Stephan-like problem for B-diffusion between moving boundaries, solving (numerically) Fick's 2nd law for B but still using steady-state approximation for the vacancy flux. Next Model 4 (Appendix A) is the most rigorous one (but most complicated and time consuming). Here we solve numerically the set of non-steady-state diffusion equations for both vacancies and species B. We compare the results of Models 1 to 4 and conclude that in most cases Model 2 is sufficient for a rough estimate, but Model 1 may lead to wrong predictions for the case of compounds. In Section 3 we consider the case of pure B-segregation at the inner boundary. In Section IV we present the kinetic Monte Carlo (kMC) simulations of nanoshell shrinking, comparing the cases of single element and IMC nanoshell with the same average bonding energy, and also comparing the kMC results with the phenomenological analysis.

2. Models of nanovoid shrinking

As already mentioned in the introduction section, any hollow nanoparticle should shrink. The general driving force of shrinking is the same for a pure component shell (Model 1) and for a IMC-shell (Models 2–4) – a decrease of total surface energy (in other formulation – Gibbs–Thomson effect). Yet, the kinetics will be different. The main differences are (1) segregation of fast diffusant at inner surface due to the inverse Kirkendall effect, and (2) the resulting decrease of vacancy flux and of corresponding shrinking rate. In general, the problem of interdiffusion within a region with moving boundaries is rather complicated for rigorous solution. So, we try to find a simplified model, which should be effective, but on the other hand, should not lose the main feature of the full process. The main simplifications are the steady-state approximations for the fluxes of vacancies and atoms. So, we present here various models with increasing degree of complexity, and then find out which model can be regarded as optimal for practical use for a given specific case.

2.1. *Model 1: shrinking of pure element nanoshells*

The vacancy out-flux is generated by the difference of equilibrium vacancy concentrations at two curved boundaries (figure 1). Vacancies are the only independent diffusing species in this case. The equation governing the vacancy concentration C_V (fraction of vacant sites) inside the shell is:

$$\frac{\partial C_V}{\partial t} = -\frac{1}{r^2}\frac{\partial}{\partial r}\left(r^2 \Omega J_V\right) + 0, \quad r_i(t) < r < r_e(t). \tag{3}$$

J_V is a vacancy flux density, Ω is an atomic volume.

The term "+0" in equation (3) is just to indicate that vacancies in our model are generated and annihilated only at the inner and external surfaces of shell. We do not consider any vacancy sinks/sources (dislocation kinks) inside the nanoshell.

The vacancy flux is governed by Fick's first law:

$$\Omega J_V = -D_V \frac{\partial C_V}{\partial r}. \tag{4}$$

Boundary conditions for vacancies were formulated by equation (2).

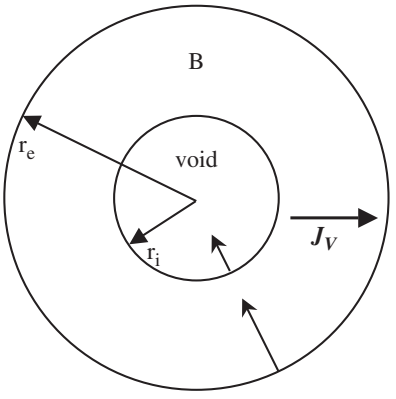

Figure 1. Scheme of pure element shell shrinking.

Inner shell/vacuum (or inert medium) and external surfaces move due to vacancy fluxes:

$$\frac{dr_i}{dt} = -\Omega J_V(r_i) = D_V \frac{\partial C_V}{\partial r}(r = r_i), \tag{5}$$

$$\frac{dr_e}{dt} = -\Omega J_V(r_e) = D_V \frac{\partial C_V}{\partial r}(r = r_e). \tag{6}$$

In steady-state approximation,

$$\frac{\partial C_V}{\partial t} \approx 0 = -\frac{1}{r^2}\frac{\partial}{\partial r}\left(r^2 \Omega J_V\right), \tag{7}$$

which leads to:

$$\Omega J_V(r_i) = -D_V \frac{\partial C_V}{\partial r} = \frac{K_V}{r^2}, \tag{8}$$

so that

$$C_V(r) = \frac{K_V}{D_V r} + M_V, \tag{9}$$

with $K_V(t)$, $M_V(t) = const$ with respect to r.

Substituting solution equation (9) into the Gibbs–Thomson boundary conditions of equation (2), we obtain:

$$K_V = C_V^{eq} \cdot D_V \cdot \beta \cdot \frac{r_e + r_i}{r_e - r_i} = D^* \cdot \beta \cdot \frac{r_e + r_i}{r_e - r_i}, \tag{10}$$

with D^* being the self diffusivity of the pure element B.

Substituting the expression of equation (10) into equations (5) and (6) for the boundary movement, we obtain the simple equations for the shrinking kinetics:

$$\frac{dr_i}{dt} = -\frac{D^*\beta}{r_i^2} \cdot \frac{r_e + r_i}{r_e - r_i}, \tag{11}$$

$$\frac{dr_e}{dt} = \frac{D^*\beta}{r_e^2} \cdot \frac{r_e + r_i}{r_e - r_i}. \tag{12}$$

Equations (11) and (12) are not independent and contain already the conservation of matter (and volume):

$$r_e^3 = r_i^3 + r_f^3. \tag{13}$$

Even this simple set of equations (11) and (12) can be solved only numerically.

To obtain an analytical estimate, we will use further assumptions. Let

$$\Delta r \equiv r_e - r_i \ll r_i. \tag{14}$$

Then conservation of volume gives

$$\Delta r \approx \frac{r_{i0}^2}{r_i^2} \Delta r_0. \tag{15}$$

Substitution of equation (15) into equation (11) and taking account of equation (13) gives:

$$\frac{dr_i}{dt} \approx -\frac{2D^*\beta}{r_{i0}^2 \Delta r_0} r_i, \tag{16}$$

which provides a shrinking behaviour of the inner radius for the initial stage of shrinking:

$$r_i(t) \approx r_i^0 \cdot \exp\left[-\frac{2D^*\beta}{r_{i0}^2 \Delta r_0} t\right]. \tag{17}$$

An approximate shrinking time follows from equation (17)

$$t_{collapse} \approx \frac{r_{i0}^2 \Delta r_0}{2D^*\beta} = \frac{kT}{4\gamma\Omega} \frac{r_{i0}^2 \Delta r_0}{D^*}. \tag{18}$$

Conservation of matter relates the initial parameters of the nanoshell with the radius r_f of resulting nanoparticle after the collapse of the nanoshell:

$$r_{i0}^2 \Delta r_0 \approx \frac{r_f^3}{3}. \tag{19}$$

So, finally,

$$t_{collapse} \approx \frac{kT}{12\gamma\Omega} \frac{r_f^3}{D^*}. \tag{20}$$

To estimate the time of collapse of a nanoshell, we take typical parameters $r_f = 4\,\text{nm}$, $\gamma = 0.5\,\text{J/m}^2$, $\Omega = 4 \cdot 10^{-29}\,\text{m}^3$, $D_A^* = 3.25 \cdot 10^{-8} \exp(-(1.24\,\text{eV}/kT))\ \text{m}^2/\text{s}$ and we found that:

$$T = 300\,\text{K} \Rightarrow t_{collapse} \approx 300 \text{ years},$$
$$T = 600\,\text{K} \Rightarrow t_{collapse} \approx 1\,\text{s}.$$

2.2. *Model 2: shrinking of a binary compound nanoshell, with steady-state approximation for both vacancies and B-species*

As already mentioned in the introduction section, the vacancy out-flux should lead to redistribution of components, i.e., segregation of the fast diffusant B atoms at the inner boundary, and segregation of the slow diffusant A atoms near the external surface (the segregation of A will be relatively less because of the larger total area of the external surface).

At first the vacancy flux, caused by difference of curvatures and corresponding vacancy concentrations, generates the inward migration fluxes J_A, J_B of both A and B species (shrinking of nanoshell). Migration of B proceeds faster, leading to segregation of B near the inner surface (figure 2). The arising concentration gradient of B influences all fluxes: it decreases the vacancy flux, suppressing the shrinking process; it also changes the fluxes of components. Here we use a phenomenological model treating a total local vacancy concentration and total local fluxes of vacancies and atoms. We don't write down separately the fluxes and concentrations at each sublattice. Different mobilities at different sublattices are taken into account implicitly, via different intrinsic diffusivities of species A and B.

2.2.1. Basic equations. The equation for the vacancies is,

$$\frac{\partial C_V}{\partial t} = -\frac{1}{r^2}\frac{\partial}{\partial r}\left(r^2 \Omega J_V\right) + 0, \quad r_i(t) < r < r_e(t) \tag{21}$$

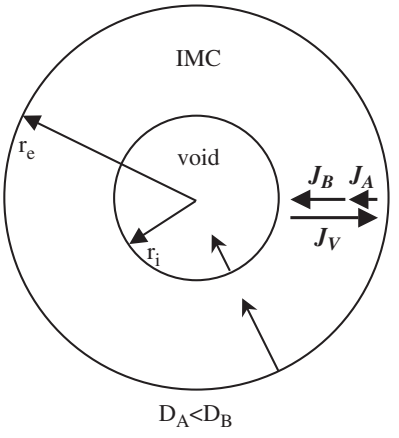

Figure 2. Scheme of IMC shell shrinking, accompanied by B-segregation at inner surface.

The equation for species B with concentration C_B (local atomic fraction of B) is,

$$\frac{\partial C_B}{\partial t} = -\frac{1}{r^2}\frac{\partial}{\partial r}\left(r^2 \Omega J_B\right), \quad r_i(t) < r < r_e(t). \tag{22}$$

Here the expressions for both fluxes should include the contributions from the vacancy gradient, in contrast to classic Darken analysis [5–8]:

$$\Omega J_V = (D_B - D_A)\frac{\partial C_B}{\partial r} - D_V \frac{\partial C_V}{\partial r}, \tag{23}$$

$$\Omega J_B = -D_B \frac{\partial C_B}{\partial r} + \frac{C_B D_B^*}{C_V}\frac{\partial C_V}{\partial r}. \tag{24}$$

All fluxes are written down in the lattice reference frame. D_B, D_B^*, D_V are, respectively, the partial diffusivity of B, the tracer diffusivity of B, and the diffusivity of vacancies inside the nanoshell. In equations (23) and (24) we have neglected Manning's corrections (vacancy wind effect). It could be done but it would make mathematical equations more cumbersome without a substantial change of the main results.

Under the same assumption, the mentioned diffusivities are interrelated in the following way:

$$\begin{aligned} &D_B = D_B^* \varphi, \quad D_A = D_A^* \varphi, \\ &\varphi = \frac{C_A C_B}{kT}\frac{\partial^2 g}{\partial C_B^2}, \\ &D_V = \frac{C_A D_A^* + C_B D_B^*}{C_V}. \end{aligned} \tag{25}$$

Here φ is a thermodynamic factor, g is Gibbs free energy per atom.

As in Model 1, the inner and external surfaces move due to vacancy fluxes:

$$\frac{dr_i}{dt} = -\Omega J_V(r_i) = (D_B - D_A)\frac{\partial C_B}{\partial r}(r = r_i) - D_V \frac{\partial C_V}{\partial r}(r = r_i), \tag{26}$$

$$\frac{dr_e}{dt} = -\Omega J_V(r_e) = (D_B - D_A)\frac{\partial C_B}{\partial r}(r = r_e) - D_V \frac{\partial C_V}{\partial r}(r = r_i). \tag{27}$$

Boundary conditions for vacancies were formulated by equation (2). Conservation of atoms of B implies that the flux of B across the moving boundaries should be absent:

$$\Omega J_B(r_i) - C_B(r_i) \cdot \frac{dr_i}{dt} = 0, \tag{28}$$

$$\Omega J_B(r_e) - C_B(r_e) \cdot \frac{dr_e}{dt} = 0. \tag{29}$$

2.2.2. Main assumptions. Let the segregation be small, so that we can use C_1 instead of C_B and $1 - C_1$ instead of C_A everywhere except derivatives (C_1 – stoichiometric concentration of B in IMC).

The same is assumed for the vacancy concentration. Let $\beta/r \ll 1$, so that we can use C_V^{eq} instead of C_V everywhere, except derivatives.

The first two assumptions mean that we can treat all arising diffusivities as almost constant.

We'll use the steady-state approximation both for components and for vacancies:

$$\frac{\partial}{\partial r}\left(r^2 J_V\right) \approx 0, \quad \frac{\partial}{\partial r}\left(r^2 J_B\right) \approx 0,$$

so that

$$\Omega J_V \approx \frac{K_V}{r^2} (> 0), \quad \Omega J_B \approx \frac{K_B}{r^2} (< 0), \tag{30}$$

which immediately leads (with almost constant diffusivities) to the same type of dependence for both vacancies and component B:

$$\frac{\partial C_V}{\partial r} \approx -\frac{L_V}{r^2}, \tag{31a}$$

$$\frac{\partial C_B}{\partial r} \approx -\frac{L_B}{r^2}. \tag{31b}$$

From equation (31a) and boundary conditions equation (2) we obtain:

$$C_V = M_V + \frac{L_V}{r} \tag{32}$$

with

$$L_V = C_V^{eq} \beta \frac{1/r_i + 1/r_e}{1/r_i - 1/r_e}, \quad M_V = C_V^{eq} \cdot \left(1 - \frac{2\beta}{r_e - r_i}\right). \tag{33}$$

On the other hand, combining equations (26–31), we obtain the following set of relations between parameters K_V, K_B, L_V, L_B:

$$\begin{aligned} K_V &= -(D_B - D_A) L_B + D_V L_V, \\ K_B &= D_B L_B - (C_1 \cdot D_B^* / C_V) L_V, \\ K_B &= -K_V C_1. \end{aligned} \tag{34}$$

This set of algebraic equations, together with equation (33), has the following solution:

$$K_V = L_V \frac{D_A^* D_B^*}{C_V^{eq} \cdot [C_1 \cdot D_A^* + (1 - C_1) D_B^*]} = \frac{D_A^* D_B^*}{C_1 \cdot D_A^* + (1 - C_1) D_B^*} \beta \frac{1/r_i + 1/r_e}{1/r_i - 1/r_e}, \tag{35}$$

$$K_B = -\frac{C_1 \cdot D_A^* D_B^*}{C_1 \cdot D_A^* + (1 - C_1) D_B^*} \beta \frac{1/r_i + 1/r_e}{1/r_i - 1/r_e}, \tag{36}$$

$$L_B = \frac{1}{\varphi} \frac{C_1 \cdot (1 - C_1)(D_B^* - D_A^*)}{C_1 \cdot D_A^* + (1 - C_1) D_B^*} \beta \frac{1/r_i + 1/r_e}{1/r_i - 1/r_e}. \tag{37}$$

To obtain parameters of B-component redistribution,

$$C_B - C_1 = M_B + \frac{L_B}{r}, \tag{38}$$

we should take the conservation of matter into account:

$$\int_{r_i}^{r_e} (C_B(r) - C_1) r^2 dr = 0. \tag{39}$$

Substituting equation (38) into equation (39), we obtain:

$$M_B = -\frac{3}{2} L_B \frac{r_e^2 - r_i^2}{r_e^3 - r_i^3} = \frac{1}{\varphi} \frac{C_1 \cdot (1 - C_1)(D_B^* - D_A^*)}{C_1 \cdot D_A^* + (1 - C_1) D_B^*} \beta \frac{(r_e + r_i)^2}{(r_e - r_i)(r_e^2 + r_i^2 + r_e r_i)}. \tag{40}$$

Thus, the main results of Model 2 are the following:

The kinetics of shrinking is governed by the slow component diffusion ($D_A^* \ll D_B^*$):

$$\frac{dr_i}{dt} = -\frac{D_A^*}{1 - C_1 + C_1 \cdot (D_A^*/D_B^*)} \frac{r_e + r_i}{r_e - r_i} \cdot \frac{\beta}{r_i^2} \approx -\frac{D_A^*}{1 - C_1} \frac{r_e + r_i}{r_e - r_i} \cdot \frac{\beta}{r_i^2}, \tag{41}$$

$$\frac{dr_e}{dt} = -\cdot \frac{r_i^2}{r_e^2} \frac{dr_i}{dt}. \tag{42}$$

Vacancy distribution across the shell is:

$$C_V = C_V^{eq} \cdot \left(1 - \frac{2\beta}{r_e - r_i} + \frac{\beta}{r} \frac{r_e + r_i}{r_e - r_i}\right). \tag{43}$$

Redistribution of component B across the shell is:

$$C_B(r) - C_1 = \frac{C_1 \cdot (1 - C_1)}{\varphi} \frac{(D_B^* - D_A^*)}{C_1 \cdot D_A^* + (1 - C_1) D_B^*} \frac{r_e + r_i}{r_e - r_i} \cdot \left(\frac{\beta}{r} - \frac{3\beta}{2} \frac{r_e^2 - r_i^2}{r_e^3 - r_i^3}\right). \tag{44}$$

In full analogy with Model 1 we can obtain a rough estimate for the shrinking time:

$$t_{collapse} \approx \frac{kT}{12(1 - C_1)\gamma\Omega} \frac{r_f^3}{D^*} \quad \text{with} \quad D^* \equiv \frac{D_A^* D_B^*}{C_1 \cdot D_A^* + (1 - C_1) D_B^*}. \tag{45}$$

Characteristic profiles of $C_V(r)/C_V^{eq}$ and $C_B(r)$ are shown in figure 3.

Time dependencies of inner and external radii (typical example is presented in figure 4) were calculated up to some minimal radius (in our case it was 3β), since with the inner radius tending to zero, the accuracy of the finite difference method becomes poor. We can stop the calculation earlier, since the late stage of shrinking is very fast (collapse) due to the inverse dependence of the rate on the inner radius. Thus, time of full collapse is practically equal to the time of shrinking to the abovementioned minimal radius.

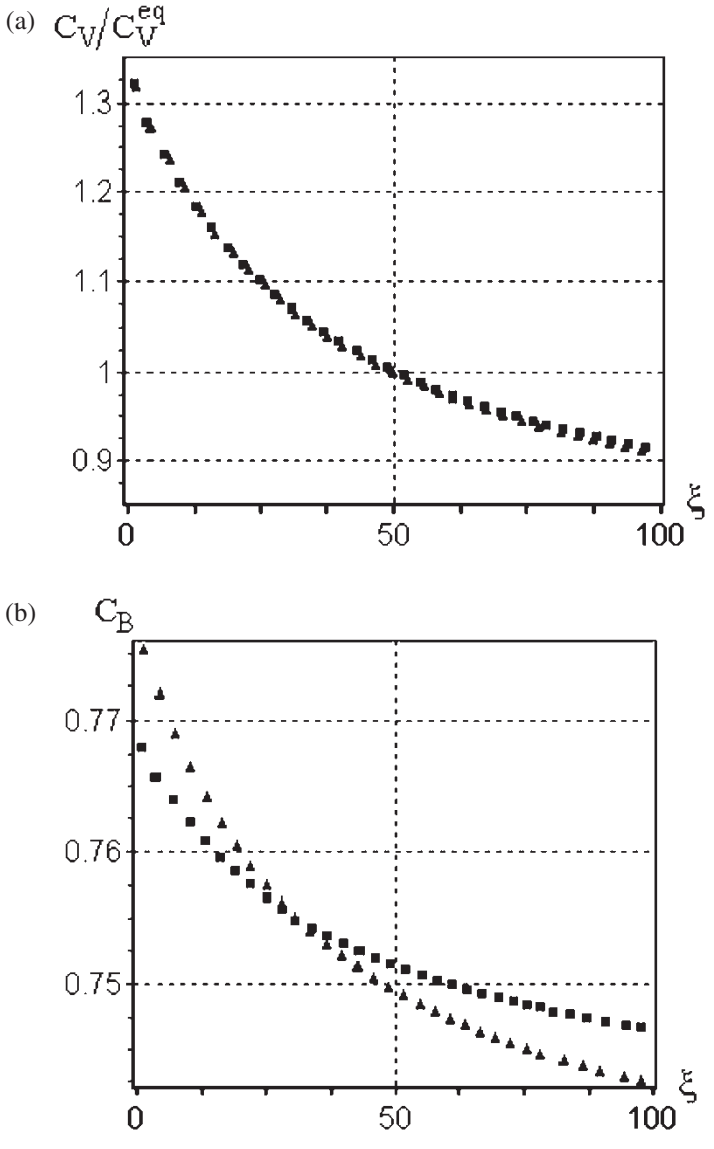

Figure 3. Redistribution of vacancies (a) and B-species (b) inside shell, calculated with Models 2 (squares) and Model 3 (triangles). Nondimensional space coordinate is $\xi = (r - r_i/r_e - r_i) \cdot 100$. (a) profiles of $C_V(r)/C_V^{eq}$ practically coincide; (b) profiles of $C_B(r)$ inside shell for models 2 and 3 differ substantially but not by order of magnitude.

Dependencies of the collapse time on the ratio D_B^*/D_A^* at initial reduced sizes $r_i/\beta = 10$, 11, 12, 13, 14, 15 are shown in figure 5. Dependencies of the collapse time on the initial inner radius r_i/β at $D_B^*/D_A^* = 10$, 20, 40, 60, 80, 100 are shown in figure 6.

Figures 5 and 6 demonstrate that the rough approximation of shrinking time in equation (45) is quite reasonable.

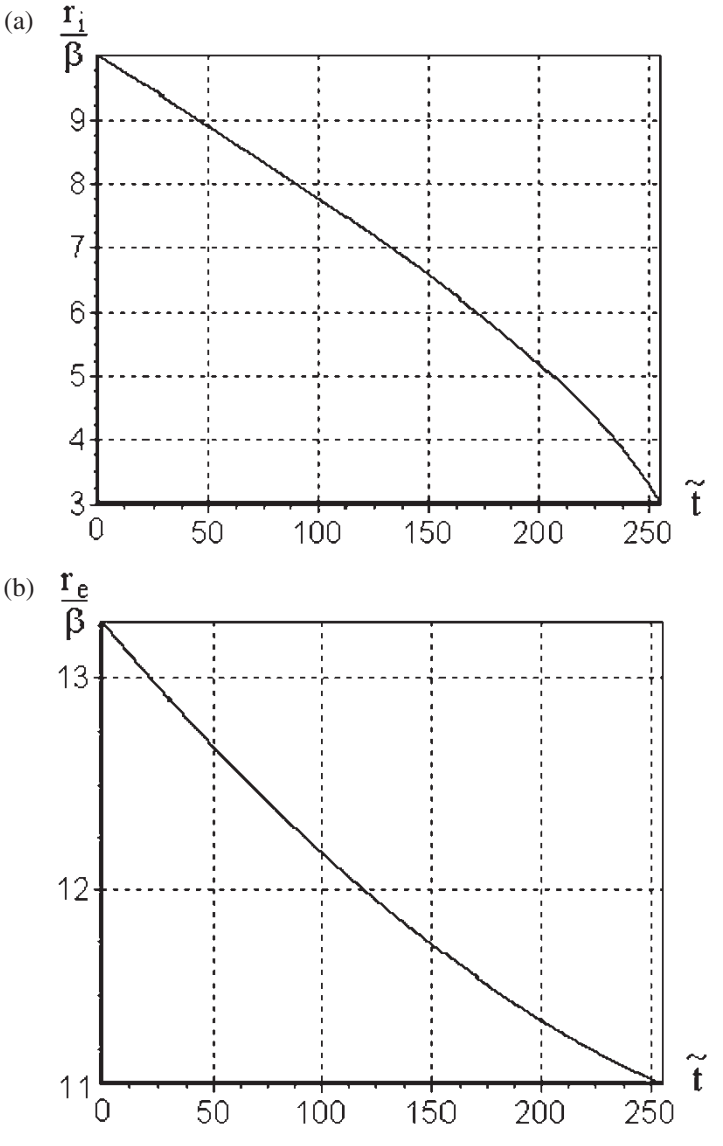

Figure 4. Time dependencies of inner (a) and external (b) radii according to Model 2. Nondimensional time is $\tilde{t} = (D_B^* t/\beta^2)$. Characteristic size β was introduced in equation (2).

2.3. *Model 3: steady-state vacancies and non-steady-state for component B*

In this model we shall still use the steady-state approximation for vacancies but will solve the non-steady-state diffusion equation for the redistribution of component B between the moving surfaces.

2.3.1. Basic equations. As in Models 1 and Model 2, we have $(\partial/\partial r)(r^2 J_V) \approx 0$, so that $\Omega J_V \approx (K_V/r^2)$ (>0). Yet, we do not have similar equations for B.

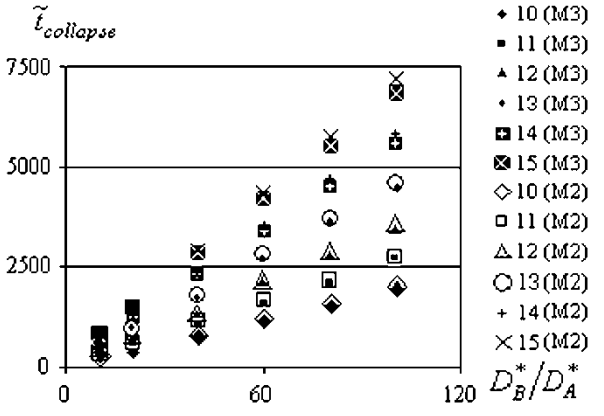

Figure 5. Dependence of nondimensional collapse time $\tilde{t}_{collapse} = (D_B^* t_{collapse}/\beta^2)$ on the ratio of diffusivities D_B^*/D_A^* for models 2 and 3 at different initial nanoshell sizes (r_{i0}/β). (For example, 11(M3) corresponds to the collapse time dependence on D_B^*/D_A^*, calculated for initial size $(r_{i0}/\beta) = 11$). Difference is small in all cases.

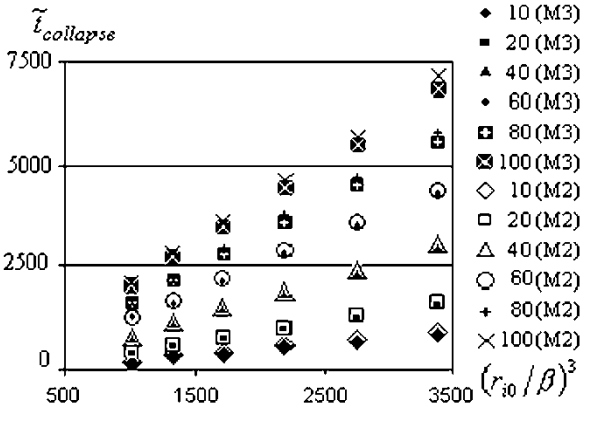

Figure 6. Dependence of nondimensional collapse time on cubed initial nanoshell sizes $(r_{i0}/\beta)^3$ for models 2 and 3 at various ratios of diffusivities D_B^*/D_A^*. (For example, 20(M3) corresponds to the collapse time dependence on $(r_{i0}/\beta)^3$ calculated for the ratio of diffusivities $D_B^*/D_A^* = 20$). Difference is small in all cases.

Therefore, in this more general case, equation (23) transforms into

$$\frac{\partial C_V}{\partial r} = \frac{D_B - D_A}{D_V}\frac{\partial C_B}{\partial r} - \frac{K_V}{D_V}\frac{1}{r^2}. \tag{46}$$

Let, as in Model 2, D_A, D_B, D_V, φ be approximately constant inside the nanoshell with narrow homogeneity range. Integrating equation (46) over all possible radii inside the nanoshell, we obtain the relation between the growth rate parameter K_V and the boundary values of the B-concentration:

$$K_V = C_V^{eq} \cdot D_V \cdot \beta \cdot \frac{r_e + r_i}{r_e - r_i} - \frac{(D_B - D_A)(C_B(r_e) - C_B(r_i))}{1/r_i - 1/r_e}. \tag{47}$$

On the other hand, integrating equation (46) over r from the inner radius to some arbitrary value, we obtain the interrelation between vacancy and B redistributions:

$$C_V(r) = C_V(r_i) + \frac{D_B - D_A}{D_V} \cdot (C_B(r) - C_B(r_i)) + \frac{K_V}{D_V}\left(\frac{1}{r} - \frac{1}{r_i}\right). \tag{48}$$

By combining equation (24) and equation (46), we get:

$$\Omega J_B = -\frac{D_A^* D_B^* \varphi}{C_1 \cdot D_B^* + (1 - C_1) D_A^*} \frac{\partial C_B}{\partial r} - \frac{C_1 \cdot D_B^*}{C_1 \cdot D_B^* + (1 - C_1) D_A^*} \frac{K_V}{r^2}. \tag{49}$$

Then equation (23) for the redistribution of B with steady-state vacancies becomes rather simple:

$$\begin{aligned} \frac{\partial C_B}{\partial t} &= D_{NG} \frac{1}{r^2} \frac{\partial}{\partial r}\left(r^2 \frac{\partial C_B}{\partial r}\right), \quad r_i(t) < r < r_e(t) \\ D_{NG} &= \frac{D_A^* D_B^* \varphi}{C_1 \cdot D_B^* + (1 - C_1) D_A^*}. \end{aligned} \tag{50}$$

For boundary conditions and for boundaries movement we obtain, using equations (26)–(29):

$$\begin{aligned} \left.\frac{\partial C_B}{\partial r}\right|_{r_i} &= -\frac{K_V}{r_i^2 D_{NG}} C_1 \cdot (1 - C_1) \frac{D_B^* - D_A^*}{C_1 \cdot D_A^* + (1 - C_1) D_B^*} \\ &= -\frac{K_V}{r_i^2} C_1 \cdot (1 - C_1) \frac{D_B^* - D_A^*}{\varphi D_A^* D_B^*}, \end{aligned} \tag{51}$$

$$\left.\frac{\partial C_B}{\partial r}\right|_{r_e} = -\frac{K_V}{r_e^2} C_1 \cdot (1 - C_1) \frac{D_B^* - D_A^*}{\varphi D_A^* D_B^*}. \tag{52}$$

Thus the smaller the ratio D_A^*/D_B^*, the sharper is the segregation at the boundaries.

Shrinking kinetics is governed by the next equations:

$$\frac{dr_i}{dt} = -\frac{K_V}{r_i^2}, \quad \frac{dr_e}{dt} = -\frac{r_i^2}{r_e^2} \frac{dr_i}{dt}, \tag{53}$$

with K_V being determined in equation (47) and dependent on sizes and compositions at interfaces.

Equation (47) and (50)–(53) form a full set for a "Stephan-like" problem with diffusion between two moving boundaries in spherically symmetrical shell. A direct solution (even a numerical one) is complicated, due to the problem of changing grid. So, we propose below to change variables, making equations somewhat cumbersome, but fixing the grid:

$$x = \frac{r - r_i(t)}{r_e(t) - r_i(t)}, \quad \tau = C_V^{eq} \frac{Bt}{\beta^2}, \quad \rho_i = \frac{r_i}{\beta}, \quad \rho_e = \frac{r_e}{\beta}. \tag{54}$$

Here $B = (D_B^*/C_V)$, which we take as constant, which appears to be a reasonable assumption for an ordered, nearly stoichiometric phase.

Let $A = (D_A^*/C_V)$, so that

$$D_V = C_A A + C_B B. \tag{55}$$

The new variable x belongs to the interval $(0, 1)$. Moving boundaries now correspond to $x = 0$ and $x = 1$. Due to the transformation of derivatives we get

$$\frac{\partial}{\partial r} = \frac{1}{\beta(\rho_e - \rho_i)}\frac{\partial}{\partial x}, \quad \frac{\partial}{\partial t} = \frac{B}{\beta^2}\left(\frac{\partial}{\partial \tau} - \left((1-x)\frac{d\rho_i}{d\tau} + x\frac{d\rho_e}{d\tau}\right)\Big/(\rho_e - \rho_i)\frac{\partial}{\partial x}\right). \tag{56}$$

The equations become more extended, but they are now suitable for numeric solution using the fixed grid. The equation for redistribution of species B within interval $0 < x < 1$ reads:

$$\frac{\partial C_B(\tau,x)}{\partial \tau} = \left((1-x)\frac{d\rho_i}{d\tau} + x\frac{d\rho_e}{d\tau}\right)\Big/(\rho_e - \rho_i)\frac{\partial C_B}{\partial x} + \frac{1}{(\rho_e - \rho_i)^2 \cdot [(\rho_e - \rho_i)x + \rho_i]^2}\frac{\partial}{\partial x}\left\{[(\rho_e - \rho_i)x + \rho_i]^2 \cdot \left[dng \cdot \frac{\partial C_B}{\partial x}\right]\right\} \tag{57}$$

with $dng = \varphi((A/B)/(C_1 + (1 - C_1) \cdot A/B))$.

In non-dimensional units the shrinking rates are:

$$\frac{d\rho_i}{d\tau} = -\frac{\tilde{K}_V}{\rho_i^2}, \quad \frac{d\rho_e}{d\tau} = -\frac{\tilde{K}_V}{\rho_e^2}. \tag{58}$$

For $\tilde{K}_V$ the expression

$$\tilde{K}_V = dv\frac{\rho_e + \rho_i}{\rho_e - \rho_i} - \varphi\frac{(1 - A/B)(C_B(x=1) - C_B(x=0))}{1/\rho_i - 1/\rho_e}. \tag{59}$$

The boundary conditions are:

$$\left.\frac{\partial C_B}{\partial x}\right|_0 = -\frac{\tilde{K}_V}{(\rho_e - \rho_i)\rho_i^2} C_1 \cdot (1 - C_1)\frac{1 - A/B}{\varphi A/B}, \tag{60}$$

$$\left.\frac{\partial C_B}{\partial x}\right|_1 = -\frac{\tilde{K}_V}{(\rho_e - \rho_i)\rho_e^2} C_1 \cdot (1 - C_1)\frac{1 - A/B}{\varphi A/B}. \tag{61}$$

Comparison of the numerical solution for Model 3 and the analytical solution for the less rigorous Model 2 is represented in figures 5 and 6. This comparison demonstrates that in most cases Model 2 is quite good for practical estimates. The most rigorous Model 4 with non-steady-state equations for both vacancies and component B is briefly reviewed in Appendix A.

3. Segregation of pure B at the inner surface

We can see from the results of Model 2 and Model 3 that, with decreasing inner radius, the segregation of the fast diffusant B increases. Sooner or later it can exceed the homogeneity range of the intermediate phase, which could lead to precipitation of the almost pure B-phase at the inner surface. Formally, to conserve the spherical symmetry, after the precipitation the nanoshell should consist of two subshells – pure B inside, and inhomogeneous IMC outside. Thus, we would have three interfaces instead of two – void/pure B, pure B/IMC and IMC/media.

Yet, this scenario seems to be highly improbable. More probable is that the pure B will precipitate as one or few tiny pieces in the remaining void, adjacent to the IMC shell, as depicted in figure 7. With time the residual void will disappear, and we obtain pure B inside the inhomogeneous IMC-shell. After some time the partial homogenization of IMC will proceed, leaving the nonzero difference of composition between the inner and the external interface due to the curvature effect.

Yet, the most probable scenario is much simpler. The decrease of the inner radius, simultaneously with increasing segregation, causes the shift of the equilibrium boundary concentration of B inside IMC at the curved interface between B and IMC. Let us compare these two equilibrium concentrations. According to standard thermodynamics at curved interfaces, the mentioned shift is equal to

$$\Delta C_B(r_i) = \frac{2\gamma_{B/IMC}\Omega}{g''_{IMC}(1-C_1)}\frac{1}{r_i}. \tag{62}$$

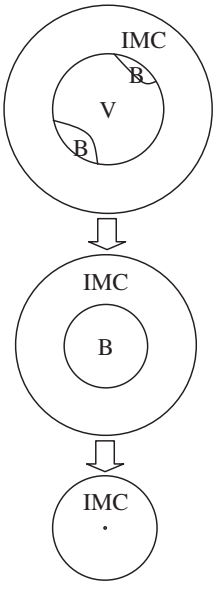

Figure 7. Possible scheme of precipitation of B at inner interface. Amount of precipitated B is schematically exaggerated.

On the other hand, according to equation (44), even for diffusivity of A tending to zero, the segregation at the inner boundary is less than

$$C_B(r) - C_1 = \frac{1}{g''_{IMC}(1-C_1)} \frac{r_e + r_i}{r_e - r_i} \cdot \frac{2\gamma_{void/IMC}\Omega}{r_i}. \tag{63}$$

The difference between equation (63) and equation (62) may be positive, meaning precipitation, but the absolute value of super-saturation will be very small, taking into account usually the large second derivatives of Gibbs potential over concentration (g'') for a highly ordered intermetallic phase. Thus, we expect that the segregation cannot exceed the size-dependent homogeneity range too much, and the precipitation of B, if attainable at all, will be small.

4. Kinetic Monte Carlo simulation of shrinking of a nanoshell

Analyses presented in the previous sections are purely phenomenological and do not take into account the possible peculiarities of diffusion and structure changes in nanoparticles. It is important to check the main ideas of shrinking of a nanoshell by direct kinetic Monte Carlo simulation.

We have simulated the nanoshell behavior for two cases: (1) pure component B with FCC lattice in vacuum in subsection 4.1; (2) an ordered FCC phase of initially homogeneous composition A_1B_3 in vacuum in subsection 4.2.

Basic algorithm

We consider pair interactions only with nearest neighbors. To compare the rates of shrinking of pure B (case (1)) and of IMC (cases (2), (3)), we used a constraint of equal average pair energy in the random alloy approximation:

$$C_A^2\Phi_{AA}^{IMC} + 2C_AC_B\Phi_{AB}^{IMC} + C_B^2\Phi_{BB}^{IMC} = \Phi_{BB}^{pure}. \tag{64}$$

Namely, we have chosen the following pair energies: $(\Phi_{BB}^{pure}/kT) = -0.414$ for case (1) and $(\Phi_{AA}^{IMC}/kT) = -0.18045$, $(\Phi_{AB}^{IMC}/kT) = -0.8$, $(\Phi_{BB}^{IMC}/kT) = -0.2$ for case (2).

Different pre-exponential frequencies ν_{0A}, ν_{0B}, are introduced for A and B species. Candidate for the jumping atom is chosen randomly from the array consisting of N_A A-atoms and $(\nu_B/\nu_A)N_B$ B-atoms. Since we have a large number of surface atoms, often an atom has several ($0 \le Z \le 12$) possible jump directions. For each of them the difference of energies after jump and before jump is calculated. $Z+1$ events are possible – jump into one of Z empty site or no jump at all (staying in site). Probabilities of these events are calculated [10, 11] as:

$$p(i) = \exp\left(-\frac{E^{after}(i) - E^{before}(i)}{kT}\right) \Bigg/ \left[\sum_{j=1}^{Z} \exp\left(-\frac{E^{after}(j) - E^{before}(j)}{kT}\right) + 1\right], \quad i = 1,\ldots,Z, \tag{65}$$

$$p(stay) = 1 \Bigg/ \left[\sum_{j=1}^{Z} \exp\left(-\frac{E^{after}(j) - E^{before}(j)}{kT}\right) + 1\right]. \tag{66}$$

4.1. *Pure B-shell in vacuum*

There are 76662 atoms of B initially to form a nanoshell with FCC lattice, with inner radius $r_i = 7a$ (a – lattice parameter) and external radius $r_e = 17a$. No initial vacancies were introduced in the nanoshell. They started coming into the nanoshell from the vacuum. Rather soon the faceting of the inner void became observable, though not very pronounced at the given energy/temperature and sizes. As expected, the void started shrinking due to clearly observable vacancy out-flux. The whole shell collapsed after 3650 Monte-Carlo steps (MCS). Three snapshots (''equatorial'' cross-sections of the simulated 3D-picture) are presented in figures 8(a), 8(b), 8(c). Change of external radius is hard to detect since at given parameters (even neglecting newly formed vacancies) it is approximately equal to $\Delta r_e/r_e \cong (r_i/r_e)^3/3$ and is less than 2.4%.

4.2. *Ordered IMC-nanoshell in vacuum*

An ideally ordered A_1B_3 compound nanoshell with FCC lattice was initiated, and there were no vacancies within the nanoshell. Initial sizes were the same as for the pure B (case (1)). KMC simulations confirm that:

- Shrinking is much slower for a compound shell compared with a pure element shell (figure 8e, 8f).
- The fast diffusant can indeed segregate at the inner surface, but the segregation is small.
- The order is basically conserved during shrinking.

5. Summary

(1) Nanoshells, produced in the diffusive reactions of nanoparticles with ambient with simultaneous formation of Kirkendall voids inside, are unstable in principle, but the shrinking time can be very large due to its cubical

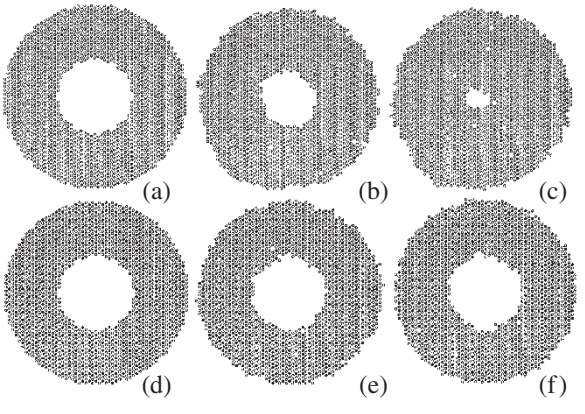

Figure 8. Snapshots of nanoshell shrinking in vacuum: top (a,b,c) – pure element nanoshell, bottom (d,e,f) – compound nanoshell (only ''equatorial'' cross-sections are given). (a,d) – initial configuration, (b,e) – after 1800 MCS, (c,f) – after 3600 MCS.

dependence on the radius of the nanoparticle. Mechanism of shrinking is the out-diffusion of vacancies from the void due to curvature effect.
(2) Shrinking of a nanoshell of intermetallic compound with a large difference between diffusivities of components is accompanied by segregation of the fast diffusant at the inner boundary due to the inverse Kirkendall effect.
(3) The rate of shrinking is controlled by the slow species, contrary to usual interdiffusion with quasiequilibrium vacancies.
(4) The steady-state approximation for both vacancies and atoms provides a reasonable and simple scheme for predicting the shrinking kinetics.
(5) In order to properly describe the details of segregation, one must take into account the non-steady state redistribution of atoms, but the steady-state for vacancies can be used.
(6) Kinetic Monte Carlo simulations confirm the main predictions of the phenomenological models.

Acknowledgements

This work was supported by Civilian Research and Development Foundation (grant #UE1-2523-503736) and in part by Ministry of Education and Science of Ukraine. AMG and TVZ are grateful to Department of Materials Science and Engineering at UCLA for their hospitality.

Appendix A: Model 4. Non-steady-state redistribution of vacancies and atoms

Basic equations:

$$\frac{\partial C_V}{\partial t} = \frac{1}{r^2}\frac{\partial}{\partial r}\left(r^2\left[-(D_B - D_A)\frac{\partial C_B}{\partial r} + D_V\frac{\partial C_V}{\partial r}\right]\right), \tag{A1}$$

$$\frac{\partial C_V}{\partial t} = \frac{1}{r^2}\frac{\partial}{\partial r}\left(r^2\left[D_B\frac{\partial C_B}{\partial r} - \frac{C_B D_B^*}{C_V}\frac{\partial C_V}{\partial r}\right]\right), \tag{A2}$$

$$\frac{dr_i}{dt} = \left[\frac{D_A D_B}{(C_A D_B + C_B D_A)\varphi}\cdot\frac{1}{C_V}\cdot\frac{\partial C_V}{\partial r}\right]_{r=r_i}, \tag{A3}$$

$$\frac{dr_e}{dt} = \left[\frac{D_A D_B}{(C_A D_B + C_B D_A)\varphi}\cdot\frac{1}{C_V}\cdot\frac{\partial C_V}{\partial r}\right]_{r=r_e}, \tag{A4}$$

$$\frac{\partial C_B}{\partial r}(r_i) = \left[C_A C_B\frac{D_B - D_A}{(C_A D_B + C_B D_A)\varphi}\cdot\frac{1}{C_V}\cdot\frac{\partial C_V}{\partial r}\right]_{r=r_i}, \tag{A5}$$

$$\frac{\partial C_B}{\partial r}(r_e) = \left[C_A C_B\frac{D_B - D_A}{(C_A D_B + C_B D_A)\varphi}\cdot\frac{1}{C_V}\cdot\frac{\partial C_V}{\partial r}\right]_{r=r_e}, \tag{A6}$$

$$C_V(r_i) = C_V^{eq} \cdot \left(1 + \frac{\beta}{r_i}\right), \tag{A7}$$

$$C_V(r_e) = C_V^{eq} \cdot \left(1 - \frac{\beta}{r_e}\right). \tag{A8}$$

One can see from these equations, prior to any solution, that the shrinking rate will be controlled by the slow species diffusion. Indeed, if $D_A \ll D_B$, then

$$\frac{D_A D_B}{C_A D_B + C_B D_A} \approx \frac{D_A D_B}{C_A D_B} = \frac{D_A}{C_A}.$$

Thus, the smaller the ratio (D_A/D_B), the slower is the shrinking rate. It means that the nanoshell, though unstable in principle, can be a rather long-living object.

As in Model 3, we propose to change variables, fixing the boundaries at:

$$x = \frac{r - r_i(t)}{r_e(t) - r_i(t)}, \quad \tau = \frac{Bt}{\beta^2}, \quad \rho_i = \frac{r_i}{\beta}, \quad \rho_e = \frac{r_e}{\beta}. \tag{A9}$$

Here $B = (D_B^*/C_V)$, which we take as constant (seems to be a reasonable assumption for ordered, nearly stoichiometric phase).

We will also use $A = (D_A^*/C_V)$, so that $D_V = C_A A + C_B B$.

The new variable x belongs to the interval $(0, 1)$. Moving boundaries now correspond to $x = 0$ and $x = 1$. Thus, equations (A1–A8) are transformed into the following set:

$$\begin{aligned}\frac{\partial C_V(\tau, x)}{\partial \tau} = {} & \left((1-x)\frac{d\rho_i}{d\tau} + x\frac{d\rho_e}{d\tau}\right)\Big/(\rho_e - \rho_i)\frac{\partial C_V}{\partial x} \\ & + \frac{1}{(\rho_e - \rho_i)^2 \cdot [(\rho_e - \rho_i)x + \rho_i]^2} \\ & \times \frac{\partial}{\partial x}\left\{[(\rho_e - \rho_i)x + \rho_i]^2 \cdot \left[-\varphi\left(1 - \frac{A}{B}\right)C_V\frac{\partial C_B}{\partial x} + \left(C_B + C_A\frac{A}{B}\right)\frac{\partial C_V}{\partial x}\right]\right\}\end{aligned}$$

$$\begin{aligned}\frac{\partial C_B(\tau, x)}{\partial \tau} = {} & \left((1-x)\frac{d\rho_i}{d\tau} + x\frac{d\rho_e}{d\tau}\right)\Big/(\rho_e - \rho_i)\frac{\partial C_B}{\partial x} \\ & + \frac{1}{(\rho_e - \rho_i)^2 \cdot [(\rho_e - \rho_i)x + \rho_i]^2} \\ & \times \frac{\partial}{\partial x}\left\{[(\rho_e - \rho_i)x + \rho_i]^2 \cdot \left[\varphi \cdot C_V\frac{\partial C_B}{\partial x} - C_B\frac{\partial C_V}{\partial x}\right]\right\},\end{aligned}$$

$$\frac{d\rho_i}{d\tau} = \frac{A/B}{C_A(0) + C_B(0) \cdot A/B}\frac{\partial C_V}{\partial x}(x = 0), \quad \frac{d\rho_e}{d\tau} = \frac{A/B}{C_A(1) + C_B(1) \cdot A/B}\frac{\partial C_V}{\partial x}(x = 1),$$

$$\left.\frac{\partial C_B}{\partial x}\right|_{x=0} = C_A(0)C_B(0)\frac{1-A/B}{C_A(0)+C_B(0)\cdot A/B}\frac{1}{\varphi C_V(0)}\frac{\partial C_V}{\partial x}(x=0),$$

$$\left.\frac{\partial C_B}{\partial x}\right|_{x=1} = C_A(1)C_B(1)\frac{1-A/B}{C_A(1)+C_B(1)\cdot A/B}\frac{1}{\varphi C_V(1)}\frac{\partial C_V}{\partial x}(x=1),$$

$$C_V(X=0) = C_V^{eq}\cdot(1+1/\rho_i), \quad C_V(X=1) = C_V^{eq}\cdot(1+1/\rho_e),$$

$$\rho_i(t=0) = \rho_{i0}, \quad \rho_e(t=0) = \rho_{e0}.$$

A numeric solution of the above formulated problem confirms the main result that the time of void shrinking is approximately inversely proportional to the ratio $A/B = D_A/D_B$.

References

[1] A.D. Smigelskas and E.O. Kirkendall, Trans. AIME **171** 130 (1947).
[2] Y. Yin, R.M. Rioux, C.K. Erdonmez, *et al.*, Science **304** 711 (2004).
[3] K.N. Tu and U. Goesele, Appl. Phys. Lett. **86** 093111 (2005).
[4] I.M. Lifshitz and V.V. Slezov, Sov. JETP **35** 479 (1958).
[5] A.D. Marwick, J. Phys. **F8** 1849 (1978).
[6] A.V. Nazarov and K.P. Gurov, Fizika metallov i metallovedenie **37** 496 (1973).
[7] K.P. Gurov and A.M. Gusak, Fizika metallov i metallovedenie **59** 1062 (1985).
[8] A.M. Gusak, Materials Science Forum **155–156** 55 (1994).
[9] A.M. Gusak and K.P. Gurov, in *Proceedings of PTM-94-Solid-Solid Phase Transformations*, edited by W.C. Johnson, J.M. Howe, D.E. Laughlin, *et al.* (TMS, USA, 1994), p. 1133.
[10] A.M. Gusak, A.A. Kovalchuk and A.O. Bogatyrev, Defect and Diffusion Forum **143–147** 661 (1997).
[11] M.O. Pasichnyy and A.M. Gusak, Defect and Diffusion Forum **237–240** 1193 (2005).